arXiv:1512.03767v1 [math.CA] 11 Dec 2015

Bifurcations analysis of the twist-Fréedericksz transition in a nematic liquid-crystal cell with pre-twist boundary conditions: the asymmetric case[1]

F.P. da Costa[2], M.I. Méndez[†3], J.T. Pinto[4]

[2]Departamento de Ciências e Tecnologia, Universidade Aberta, Lisboa, Portugal, and Centro de Análise Matemática, Geometria e Sistemas Dinâmicos, Instituto Superior Técnico, Universidade de Lisboa, Lisboa, Portugal

[3]Departamento de Matemáticas, IES Antonio López, Getafe (Madrid), Spain

[4]Departamento de Matemática and Centro de Análise Matemática Geometria e Sistemas Dinâmicos, Instituto Superior Técnico, Universidade de Lisboa, Lisboa, Portugal

December 10, 2015

Abstract. In the paper [Eur. J. of Appl. Math. **20**, (2009) 269–287] by da Costa et al. the twist-Fréedericksz transition in a nematic liquid crystal one-dimensional cell of lenght L was studied imposing an antisymmetric net twist Dirichlet condition at the cell boundaries. In the present paper we extend that study to the more general case of net twist Dirichlet conditions without any kind of symmetry restrictions. We use phase-plane analysis tools and appropriately defined time-maps to obtain the bifurcation diagrams of the model when L is the bifurcation parameter, and related these diagrams with the one in the symmetric situation. The stability of the bifurcating solutions is investigated by applying the method of Kenjiro Maginu [J. Math. Anal. Appl. **63**, (1978) 224–243].

1. Introduction

In the operation of liquid crystal devices the phenomena of Fréedericksz transitions in nematic liquid crystal cells are of paramount technological importance [8, Chapter 5] and give rise to interesting and challenging mathematical problems [7, Section 3.4].

A nematic liquid crystal cell is basically a thin layer (a few microns) of a nematic liquid crystal contained between two glass plates whose inner surface is chemically treated in such a way as to force a certain allignment (anchoring) of the rod like nematic liquid crystal molecules lying close to the cell boundary. This surface alignment induces an allignment in the liquid crystal molecules filling the cell bulk so that the total free energy is minimized.

When an exterior electric or magnetic field is applied to the cell a competition takes place between the reorienting effects of the field and the allignment imposed by the surface anchoring. Minimization of the total free energy (field, elastic bulk, and anchoring) then forces a reallignment of the molecules in the cell bulk (and, in the case of the so called weak anchoring conditions, also of those at the cell surface [2]) when the field intensity increases above a threshold value dependent on the physico-chemical characteristics of the device. This bifurcation phenomenon is called Fréedericksz transition, in honor of the soviet physicist who discovered it [4].

If we model the rod-like nematic liquid crystal molecules by a "director vector field" $\mathbf{n}$, with $\|\mathbf{n}\| \equiv 1$, a system with strong anchoring of the molecules at the cell surface occupying a region Ω has a total free energy of the director field given by

$$\int_\Omega w(\mathbf{n}, \nabla \mathbf{n}),$$

where the free-energy density w embodies the competition between the energy cost of distortions of the director field versus the energy reduction associated with aligning parallel (or perpendicular) to the magnetic field, and is givem by

$$2w = K_1 \left(\operatorname{div} \mathbf{n}\right)^2 + K_2 \left(\mathbf{n} \cdot \operatorname{curl} \mathbf{n}\right)^2 + K_3 \left\|\mathbf{n} \times \operatorname{curl} \mathbf{n}\right\|^2 - \mu_0 \Delta\chi (\mathbf{H} \cdot \mathbf{n})^2,$$

where K_1, K_2, and K_3 are phenomenological elastic constants, μ_0 is the free-space magnetic permeability, $\Delta\chi = \chi_\parallel - \chi_\perp$ is the difference between the diamagnetic susceptibilities parallel to versus perpendicular to the director, and $\mathbf{H}$ is the (constant) applied magnetic field. See, e.g., [7].

We consider the geometry of the twist-Fréedericksz transition, with an asymmetric pre-twist at the boundary. Thus we consider a thin slab of nematic liquid crystal bounded by two parallel planes a distance d apart

[1]F.P. da C. and J.T.P. were partially supported by FCT/Portugal through UID/MAT/04459/2013.

[†]Portions of this paper first appeared in the dissertation submited by the second author to the *Universidad Nacional de Educación a Distancia,* Madrid, Spain, in June 2014, as part of the requirements for the degree of *Máster en Matemáticas Avanzadas.*

from each other, unbounded and extending to infinity in any direction parallel to these planes. Define a positively oriented orthogonal coordinate system (x, y, z) such that z is perpendicular to the bounding planes. Let the director field be represented by

$$\mathbf{n} = (\cos\phi(z,\tau), \sin\phi(z,\tau), 0), \tag{1.1}$$

where ϕ denotes the (twist) angle of the director. We will assume that in the liquid crystal cell the director is fixed in opposing orientations $-\phi_0$ and ϕ_1 at the two opposing planes bounding the device in the z direction. This induces a net twist of the director vector field $\mathbf{n}$ across the cell (see Figure 1).

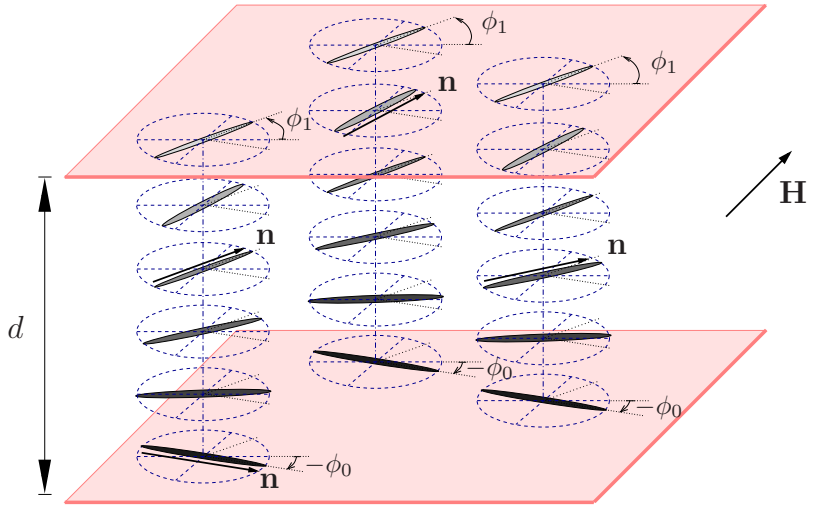

FIGURE 1. Geometry of the liquid crystal cell with asymmetric pre-twist. The director $\mathbf{n}$ orientation inside the cell corresponds to the situation in branch C_r (with $k = 0$) in Section 3.1 below.

We will consider a magnetic vector field $\mathbf{H}$ applied along the constant direction $(0, 1, 0)$ with intensity $H = \|\mathbf{H}\|$ and are interested in studying the effect it induces in the stationary director distribution, according to the Ericksen-Leslie theory [7].

In terms of the angle representation 1.1, the simplest model for the dynamics of the director field in the absence of flow is the gradient flow on the *free energy* of the system and, in dimensionless form, the initial-boundary value problem governing the behaviour of the director field is then

$$\frac{\partial\phi}{\partial s} = \frac{\partial^2\phi}{\partial\zeta^2} + \lambda\sin\phi\cos\phi, \qquad (s,\zeta) \in \mathbb{R}^+ \times (0,1) \tag{1.2}$$

$$\phi(\cdot,0) = -\phi_0, \qquad \phi(\cdot,1) = \phi_1, \tag{1.3}$$

$$\phi(0,\cdot) = \phi_{\text{initial}} \tag{1.4}$$

where

$$s := \frac{K_2}{\gamma_1 d^2}\tau \ , \quad \zeta := \frac{z}{d} \ , \quad \lambda := \frac{\mu_0\Delta\chi H^2 d^2}{K_2}, \tag{1.5}$$

with all the material parameters are positive for our system of interest. Observe that the dimensionless control parameter λ is proportional to the square of the magnetic field strength.

The associated equilibrium problem is given by

$$\frac{d^2\phi}{d\zeta^2} + \lambda\sin\phi\cos\phi = 0, \qquad 0 < \zeta < 1 \tag{1.6}$$

$$\phi(0) = -\phi_0, \quad \phi(1) = \phi_1. \tag{1.7}$$

In the classical twist-Fréedericksz-transition problem, we have $\phi_0 = \phi_1 = 0$ the system possesses a simple symmetry, $\phi(\zeta) \leftrightarrow -\phi(\zeta)$, and the ground-state solution ($\phi = 0$, which is invariant under this symmetry) loses stability to a pair of symmetric solutions at a pitchfork bifurcation at $\lambda_c = \pi^2$.

In [1] a system with antisymmetric pre-twist ($\phi_0 = \phi_1 \neq 0$) was studied. We no longer have the simple symmetry above. The problem still possesses $\mathbb{Z}_2$ symmetry, however it is now of the form $\phi(\zeta) \leftrightarrow -\phi(1-\zeta)$. The ground-state solution (which is invariant under this symmetry) is no longer uniform. The problem still has a classical pitchfork bifurcation diagram, with the symmetric solution branch bifurcating at a value λ_c,

which is necessarily greater than π^2, as was showed in [1]. Observe that the antisymmetric nature of the boundary data is crucial to this scenario.

In the present paper we consider the asymmetric case ($\phi_0 \neq \phi_1$, both nonzero). We conclude that no pitchfork bifurcation points remain: the pitchforks that had not been broken in the passage from the classical twist cenario to the antisymmetric one, are now broken when the ϕ_0 becomes different from ϕ_1, and the result is a bifurcation diagram with only saddle-node bifurcation points, branches emanating from them, and single nonbifurcating branch of solutions.

The approach will be based on the time maps and phase-plane methods developed in [1] for the antisymmetric case. The stability of these branches is also studied by applying the results of [6], also based on the behaviour of time-maps, which allows the classification of the stationary solution branches as stable, asymptotically stable, or unstable. A more detailed study of the stability indices of the equilibria and the characterization of their connecting orbits will be the subject of a future paper.

2. Preliminaries

We will be concerned with the stationary solutions to (1.2)-(1.4), i.e., solutions of (1.6)-(1.7). Consider the change of variables $t = t(\zeta) := \sqrt{\frac{\lambda}{2}}\left(\zeta - \frac{1}{2}\right)$, and let $\zeta(t)$ be its inverse function. Let

$$L := \sqrt{\frac{\lambda}{8}}. \tag{2.1}$$

Then, $\phi(\zeta)$ is a solution of (1.6)-(1.7) iff $x(t) := \phi(\zeta(t))$ is a solution of

$$\begin{cases} x' = y \\ y' = -\sin 2x \end{cases} \tag{2.2}$$

$$x(-L) = -\phi_0, \quad x(L) = \phi_1, \tag{2.3}$$

where $\phi_0, \phi_1 \in (0, \frac{\pi}{2})$, and $(t, x, y) \in [-L, L] \times [-\pi/2, \pi/2] \times \mathbb{R}$. The bifurcation parameter is now $L > 0$. Note that $L \propto H$. We shall treat the independent variable t in (2.2)-(2.3) as the "time" of the dynamical system associated with (1.2). Note that this "time" corresponds to the original spacial variable ζ and not to the original time s.

The study of the bifurcation structure of solutions to (2.2)–(2.3) when $\phi_0 = \phi_1$ was done in [1]. We now consider the general case, where no relation between the values of ϕ_0 and ϕ_1 is imposed. As in [1], we shall use the tools of time-maps and phase-plane analysis.

The phase portrait of (2.2) is presented in Figure 2.

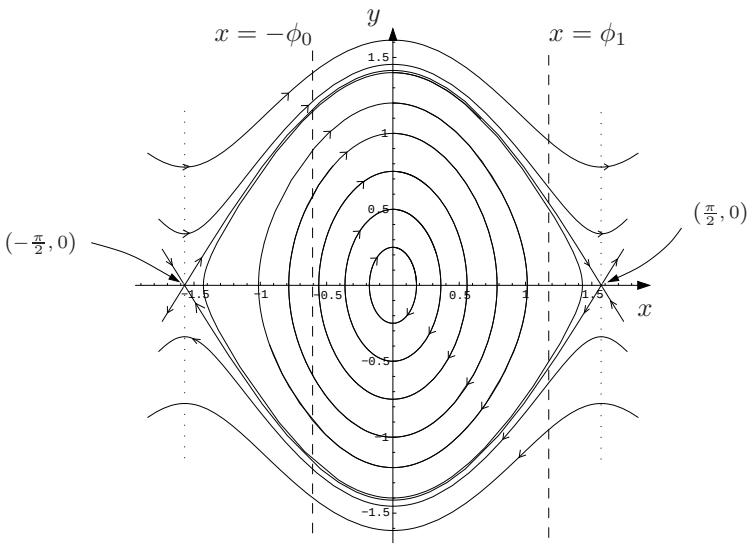

Figure 2. Orbits of (2.2) with the Dirichlet boundary condition (2.3) marked by the dashed vertical lines (with $0 < \phi_0 < \phi_1 < \pi/2$.)

For studying solutions to (2.2)-(2.3) we need to consider some time-maps measuring the time spent by the orbits. These maps are easily obtained from the fact that (2.2)-(2.3) is a conservative system with energy

$$V(x, y) = y^2 - \cos 2x, \tag{2.4}$$

which means that its orbits are subsets of the level sets of this function.

Let $\alpha \in \left(0, \frac{\pi}{2}\right)$ and denote by γ_α the orbit that, at time $t = 0$, intersects the x-axis at $(\alpha, 0)$. Clearly γ_α is a periodic orbit (cf. Figure 2). Let $P(\alpha)$ be its period and define

$$T(\alpha) := \frac{1}{4}P(\alpha) = \int_0^\alpha \frac{dx}{\sqrt{\cos 2x - \cos 2\alpha}}, \tag{2.5}$$

where the second equality arises from the symmetry of the system with respect to reflexions in the $x-$ and $y-$axis. Thus, $T(\alpha)$ is the time it takes for the point of intersection of γ_α with the $y-$axis (which, by conservation of V along orbits, we easily conclude to be the point $(0, \beta)$ with $\beta = \sqrt{2}\sin\alpha$) to reach the $x-$axis (at the point $(\alpha, 0)$, by construction).

As in [1], two other time maps will be needed. The time-map

$$T_1(\alpha, \phi) := \int_0^\phi \frac{dx}{\sqrt{\cos 2x - \cos 2\alpha}}, \tag{2.6}$$

that measures the time spent by the point of intersection of the orbit γ_α with the $y-$axis to reach the line $x = \phi \leqslant \alpha$. Clearly $T_1(\phi, \phi) = T(\phi)$. We will also consider a map T_2 analogous to T_1 but relevant for orbits crossing the $y-$axis on or above the heteroclinic orbit γ_h connecting $(-\pi/2, 0)$ to $(\pi/2, 0)$, i.e., at a point $(0, \beta)$ with $\beta \geqslant \sqrt{2}$, namely

$$T_2(\beta, \phi) := \int_0^\phi \frac{dx}{\sqrt{\beta^2 + \cos 2x - 1}}. \tag{2.7}$$

We can continuously extend this map to values $\beta < \sqrt{2}$ by $T_2(\beta, \phi) := T_1(\alpha(\beta), \phi)$, where $\alpha(\beta)$ is defined to be the unique value of α for which the points $(\alpha, 0)$ and $(0, \beta)$ are on the same orbit. Since the orbits are contained in the level sets of V, a brief inspection of Figure 2 allow us to conclude that $\beta \mapsto \alpha(\beta)$ is a monotonically increasing function and thus, for each fixed ϕ, there is a smaller β for which $T_2(\beta, \phi)$ is defined, which is the value β_ϕ for which $(\beta_\phi, 0)$ and $(\phi, 0)$ are on the same orbit. For β below β_ϕ no orbit satisfies the boundary condition at $t = L$.

Our analysis depend heavily on the following monotonicity properties of the time-maps defined above. A proof of these results can be checked in [1].

Proposition 2.1. *Let $\alpha \in \left(0, \frac{\pi}{2}\right)$, $\phi \in (0, \alpha)$, and $\beta \geqslant \beta_\phi$. Then,*

- **1:** *the time-map $T : \left(0, \frac{\pi}{2}\right) \to (0, +\infty)$ defined by (2.5) is strictly increasing and converges to $\frac{\pi}{2\sqrt{2}}$ as $\alpha \to 0$, and to $+\infty$ as $\alpha \to \frac{\pi}{2}$.*
- **2:** *for each fixed ϕ the time-maps $T_1(\cdot, \phi)$ and $T_2(\cdot, \phi)$, defined by (2.6) and (2.7), respectively, are strictly decreasing. The same holds true for $T_2(\cdot, \frac{\pi}{2})$.*

3. Bifurcation analysis

The study of (2.2)-(2.3) in the symmetric case $\phi_0 = \phi_1$ was done in [1] and will serve as a guide to our present study. In the symmetric case a special role is played by the solutions of (2.2)-(2.3) that additionally satisfy the homogeneous Neumann boundary condition $y(-L) = y(L) = 0$ (note that $y = x'$). The values of L for which these solutions occur were termed "critical" (cf. [1, Figure 4 and Table 1]) and are pitchfork bifurcation points of the system [1, Figure 9]. The orbits corresponding to these values of L were denoted by γ^*.

Due to the symmetry of the vector field of (2.2) and the asymmetry of the boundary condition (2.3) there are no solutions to (2.2)-(2.3) satisfying homogeneous Neumann boundary conditions at *both* $t = -L$ and $t = L$. However, there are solutions that satisfy such a condition at one, or the other, of the end points of the time interval. Although these do not correspond to bifurcation solutions, and the corresponding values of L are not bifurcation points of (2.2)-(2.3), they are important solutions that help us to organize the information and construct the bifurcation diagram in the asymmetric case, and relate it with the symmetric case already studied.

The two asymmetric cases $\phi_0 < \phi_1$ and $\phi_0 > \phi_1$ give rise to different bifurcation diagrams and will be studied separately below. Since the approach for both cases is the same, we will present the first one in a more detailed way, and for the second will just briefly refer to the corresponding results.

3.1. Case $\phi_0 < \phi_1$.

3.1.1. *The "critical" cases.* Let γ_* be the orbit of (2.2)-(2.3) that satisfies the additional homogeneous Neumann condition $y(L) = 0$. See Figure 3(a). It is clear from this figure and from the definition of the time-maps in the previous section that the time spent by γ_* is $T_* := T(\phi_1) + T_1(\phi_1, \phi_0)$. Since the total time spent by every orbit is $2L$, the corresponding half-length L is $L_* = \frac{1}{2}T_*$.

In a similar way, the orbit that satisfies the homogeneous Neumann boundary condition $y(-L) = 0$ will be denoted by γ^*. See Figure 3(b). The time spent in by this orbit is $T^* := 3T(\phi_1) - T_1(\phi_1, \phi_0)$, and the corresponding half-lenght of the interval is $L^* = \frac{1}{2}T^*$.

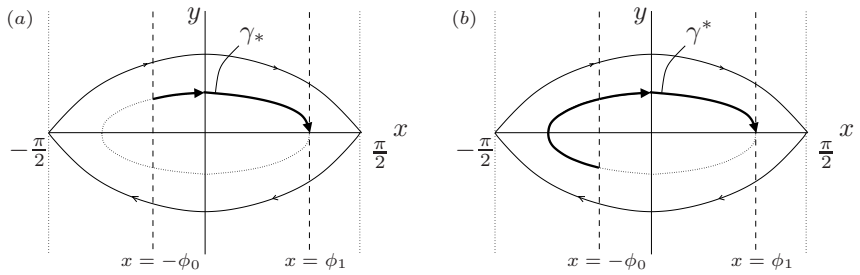

FIGURE 3. Two "critical" orbits of (2.2)-(2.3) with $\phi_0 < \phi_1$: (a) γ_* when $2L = T_* := T(\phi_1) + T_1(\phi_1, \phi_0)$; (b) γ^* when $2L = T^* := 3T(\phi_1) - T_1(\phi_1, \phi_0)$

From the definitions of the time-maps we easily observe that,

$$T_* = T(\phi_1) + T_1(\phi_1, \phi_0) < 2T(\phi_1) < 3T(\phi_1) - T_1(\phi_1, \phi_0) = T^*, \tag{3.1}$$

and these the inequalities turn to equalities if $\phi_0 = \phi_1$, which, as already pointed out, was the case considered in [1].

By analogy to the terminology used in [1] for the symmetric case we shall call these solutions, orbits, etc., "critical", although, as we shall see, they do not correspond to any critical feature in the bifurcation diagrams. However, they will be very useful for the remaining constructions. In particular, as a matter of terminology and when appropriate, we will keep denoting by subcritical [resp., supercritical] those situations with values of L smaller [resp., larger] than L^* ou L_*.

3.1.2. *The subcritical case relative to* γ_*. By Proposition 2.1 it is clear that the function $\left(\phi_1, \frac{\pi}{2}\right) \ni \alpha \mapsto T_A(\alpha) := T_1(\alpha, \phi_1) + T_1(\alpha, \phi_0)$ is monotonically decreasing and $T_A(\alpha) \uparrow T_*$ as $\alpha \downarrow \phi_1$. The corresponding orbit of (2.2)-(2.3) is a subset of the level set $V(\alpha, 0)$ of V. Since the time it spents is $2L = T_A(\alpha) < T_*$, we call it subcritical relative to γ_*. Using the relation between the time-maps T_1 and T_2 we can extend this approach to orbits intersecting the $y-$axis above the heteroclinic orbit γ_h. The time taken by these orbits is also smaller than T_* and decreases as the ordinate of the intersection point increases.

In Figure 4 we present two of these orbits subcritical relative to γ_*, together with the critical orbit γ_*. The monotonicity of the time-maps imply that, for each $L \in (0, \frac{1}{2}T_*)$ there is a single subcritical solution to (2.2)-(2.3).

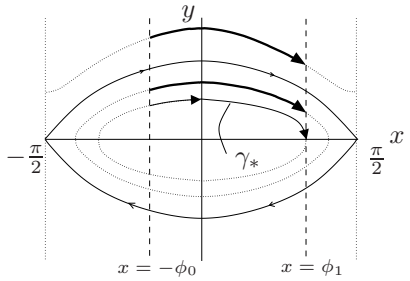

FIGURE 4. Two orbits of (2.2)-(2.3), with $\phi_0 < \phi_1$, subcritical relative to the orbit γ_*.

3.1.3. *The supercritical case relative to* γ_*. Consider again $\alpha \in \left(\phi_1, \frac{\pi}{2}\right)$ and the level set $V(\alpha, 0)$ of V. For $\alpha > \phi_1$ but close to ϕ_1, we take an orbit of (2.2)-(2.3) close to γ_* which have its end point with $y(L) < 0$, as presented in Figure 5. A brief inspection of this figure allow us to conclude that the time spent by this orbit is $T_{C_r}(\alpha) := 2T(\alpha) + T_1(\alpha, \phi_0) - T_1(\alpha, \phi_1)$ (the notation T_{C_r} was used in [1] for a branch of solutions with a given symmetry relative to the origin. We use the same notation here because our C_r solutions will coincide with those of that paper when $\phi_0 = \phi_1$; the same will be done for other solution branches further down the paper). Clearly $T_{C_r}(\alpha) \to T_*$ as $\alpha \to \phi_1$.

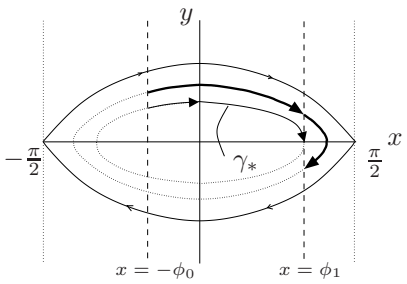

FIGURE 5. An orbit of (2.2)-(2.3), with $\phi_0 < \phi_1$, supercritical relative to the orbit γ_*.

We shall prove that $T_{C_r}(\alpha) > T_*$ for $\alpha > \phi_1$, thus providing a justification for calling these orbits supercritical relative to γ_*. From the expression of T_{C_r} and Proposition 2.1 we conclude that

$$\frac{dT_{C_r}}{d\alpha}(\alpha) = T'(\alpha) + \frac{\partial T_1}{\partial \alpha}(\alpha,\phi_0) - \frac{\partial T_1}{\partial \alpha}(\alpha,\phi_1) > \frac{\partial T_1}{\partial \alpha}(\alpha,\phi_0) - \frac{\partial T_1}{\partial \alpha}(\alpha,\phi_1). \tag{3.2}$$

To conclude the sign of the right-hand side observe that

$$\frac{\partial}{\partial \phi}\frac{\partial T_1}{\partial \alpha} = \frac{\partial}{\partial \alpha}\frac{\partial T_1}{\partial \phi} = \frac{\partial}{\partial \alpha}\frac{1}{\sqrt{\cos 2\phi - \cos 2\alpha}} = -\frac{\sin 2\alpha}{(\cos 2\phi - \cos 2\alpha)^{3/2}} < 0.$$

From this inequality and the assumption that $\phi_0 < \phi_1$ we infer that

$$\frac{\partial T_1}{\partial \alpha}(\alpha,\phi_0) > \frac{\partial T_1}{\partial \alpha}(\alpha,\phi_1),$$

and plugging this into (3.2) gives that T_{C_r} is strictly increasing with α, concluding the proof.

3.1.4. *The supercritical case relative to γ^*.* Consider an orbit in $V(\alpha,0)$, with $\alpha \in \left(\phi_1, \frac{\pi}{2}\right)$, as represented in Figure 6(a). From this figure and the definition of the time-maps we immediately conclude that the time spent to travel this orbit is $T_D(\alpha) := 4T(\alpha) - T_1(\alpha,\phi_0) - T_1(\alpha,\phi_1)$ (see subsection 3.1.3 for a justification of this notation).

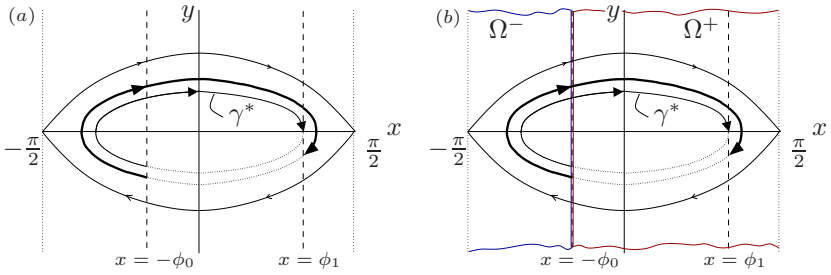

FIGURE 6. (a) An orbit of (2.2)-(2.3), with $\phi_0 < \phi_1$, supercritical relative to the orbit γ^*. (b) The Ω^- and Ω^+ regions.

Clearly $T_D(\alpha) \to T_*$ as $\alpha \to \phi_1$. We shall prove that $T_D(\alpha) > T^*$. In order to prove this, consider the strips $\Omega^- := (-\pi/2, -\phi_0) \times \mathbb{R}$, and $\Omega^+ := [-\phi_0, \pi/2) \times \mathbb{R}$. Let $\gamma^{*\pm} := \gamma^* \cap \Omega^\pm$. Denoting by D an orbit of the type represented in Figure 6, let also $D^\pm = D \cap \Omega^\pm$. Since $\gamma^{*+} = \gamma_*$, the time spent in γ^{*+} is equal to T_*.

Thus, in Ω^+ we just need to compare T_* with the time spent by D^+. But D^+ is really an orbit of type C_r with $\alpha > \phi_1$ and thus, by the previous subsection, $T_{D^+}(\alpha) > T_*$.

In Ω^- we need to compare the time taken by the orbit D^- with that taken by γ^{*-}, which a brief inspection to Figure 6(b) shows it is equal to $2T(\phi_1) - 2T_1(\phi_1,\phi_0)$. Since

$$T_{D^-}(\alpha) = 2T(\alpha) - 2T_1(\alpha,\phi_0), \quad \alpha \in (\phi_1, \pi/2),$$

we have $\frac{\partial T_{D^-}}{\partial \alpha}(\alpha) = 2T'(\alpha) - 2\frac{\partial T_1}{\partial \alpha}(\alpha,\phi_0)$, and the monotonicity results in Proposition 2.1 imply that this derivative is positive, and thus $T_{D^-}(\alpha) > 2T(\phi_1) - 2T_1(\phi_1,\phi_0)$.

Finally, from the above we have

$$\begin{aligned} T_D(\alpha) &= T_{D^-}(\alpha) + T_{D^+}(\alpha) \\ &> 2T(\phi_1) - 2T_1(\phi_1,\phi_0) + T_* = 3T(\phi_1) - T_1(\phi_1,\phi_0) \\ &= T^*, \end{aligned}$$

as we wanted to prove.

3.1.5. *The subcritical case relative to* γ^*. To complete the analysis, let us consider orbits in $V(\alpha, 0)$, with $\alpha \in \left(\phi_1, \frac{\pi}{2}\right)$, as represented in Figure 7.

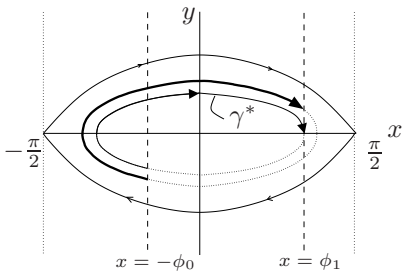

FIGURE 7. An orbit of (2.2)-(2.3), with $\phi_0 < \phi_1$, subcritical relative to the orbit γ^*.

It is clear from this plot that the time spent by this orbit is $T_{C_\ell}(\alpha) := 2T(\alpha) - T_1(\alpha, \phi_0) + T_1(\alpha, \phi_1)$ (see subsection 3.1.3 for a justification of this notation T_{C_ℓ}).

It is also clear that $T_{C_\ell}(\alpha) \to T^*$ as $\alpha \to \phi_1$. We shall prove that, for $\alpha > \phi_1$ sufficiently close to ϕ_1, we have $T_{C_\ell}(\alpha) < T^*$. This is not as easy to prove as in the previous cases. We start by considering in (2.5) and (2.6) a new variable $\tilde{\alpha} := \sin^2 \alpha$, and changing in (2.5) the integration variable $x \mapsto \theta$ where $\sin x = \sqrt{\tilde{\alpha}} \sin \theta$. This allow us to write

$$T_{C_\ell}(\alpha) = \tilde{T}_{C_\ell}(\tilde{\alpha}) := \sqrt{2} \int_0^{\pi/2} \frac{d\theta}{\sqrt{1 - \tilde{\alpha} \sin^2 \theta}} + \frac{1}{\sqrt{2}} \int_{\phi_0}^{\phi_1} \frac{dx}{\sqrt{\tilde{\alpha} - \sin^2 x}}, \tag{3.3}$$

Differentiating we obtain

$$\frac{d\tilde{T}_{C_\ell}}{d\tilde{\alpha}} = \frac{1}{\sqrt{2}} \int_0^{\pi/2} \frac{\sin^2 \theta}{\left(1 - \tilde{\alpha} \sin^2 \theta\right)^{3/2}} d\theta - \frac{1}{2\sqrt{2}} \int_{\phi_0}^{\phi_1} \frac{dx}{\left(\tilde{\alpha} - \sin^2 x\right)^{3/2}},$$

and computing the second derivative we obtain

$$\frac{d^2\tilde{T}_{C_\ell}}{d\tilde{\alpha}^2} = \frac{3}{2\sqrt{2}} \int_0^{\pi/2} \frac{\sin^4 \theta}{\left(1 - \tilde{\alpha} \sin^2 \theta\right)^{5/2}} d\theta + \frac{3}{4\sqrt{2}} \int_{\phi_0}^{\phi_1} \frac{dx}{\left(\tilde{\alpha} - \sin^2 x\right)^{5/2}} > 0.$$

Hence, $\tilde{T}_{C_\ell}$ is a convex function of $\tilde{\alpha} := \sin^2 \alpha \in (\sin^2 \phi_1, 1)$. From the definition of T_{C_ℓ} and $\tilde{T}_{C_\ell}$, the above expressions, and Proposition 2.1, we also conclude that $\tilde{T}_{C_\ell} \to +\infty$ as $\tilde{\alpha} \to 1$, and $\frac{d\tilde{T}_{C_\ell}}{d\tilde{\alpha}} \to -\infty$ as $\tilde{\alpha} \to \sin^2 \phi_1$; however, note that $\tilde{T}_{C_\ell} \to T^*$ as $\tilde{\alpha} \to \sin^2 \phi_1$ (see the start of this paragraph).

This behaviour obviously implies the existence of a single local extrema (a minimum) of $\tilde{T}_{C_\ell}$, and hence of T_{C_ℓ}, in the interior of their respetive intervals of definition, and thus $T_{C_\ell}(\alpha) < T^*$ when $\alpha > \phi_1$ sufficiently close to ϕ_1. This justifies us calling this situation a (local) subcritical case relative to γ^*. We emphasize that the situation is *local*: if α is larger than the minimizer of $T_{C_\ell}(\alpha)$, the value of this function increases without bound as $\alpha \to \pi/2$, and thus,at some point, it will certainly be larger than T^*.

Collecting the results obtained in the subsections 3.1.1–3.1.5 we obtain the bifurcation diagram in Figure 8. Remark that, due to the symmetry of the system, the value of $y(-L)$ of the orbits γ_* and γ^* have the same absolute value (and different signs).

3.1.6. *Other solution branches.* In addition to the solution branches studied above and represented in Fig. 8, (2.2)–(2.3) has an infinite number of solution families, each corresponding to orbits circling the origin a complete k number of times ($k = 1, 2, \ldots$). As in the cases studied above, it is convenient to start by considering orbits corresponding to solutions that satisfy the additional boundary condition $y(L) = 0$, and, as before, we denote those orbits by a star, in this case by γ_{*k} and γ_k^*. Although they do not correspond to bifurcating points, they are very useful in organizing or knowledge about the solution branches. In Table 1 we present the orbit γ_{*k} and those which form a connected branch with it when L changes from the value corresponding to γ_{*k}. In Table 2 we present the analogous picture concerning the orbit γ_k^*.

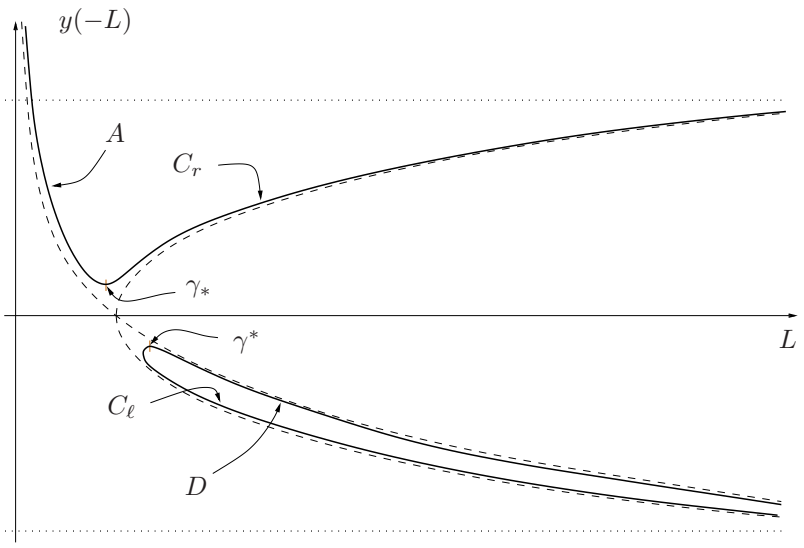

FIGURE 8. Solid lines: portion of the bifurcation diagram when $\phi_0 < \phi_1$ constructed from the analysis of the time-maps about γ_* and γ^* presented in subsections 3.1.1–3.1.5. Dashed lines: the corresponding diagram when $\phi_0 = \phi_1$ (from [1]). The designation of the orbits by letters A, C_ℓ, C_r and D correspond to those used in [1]: see Table 1 and Figure 8 of that article.

TABLE 1. Branch of solutions to (2.2)-(2.3), with $\phi_0 < \phi_1$, winding k full times around $\mathbf{0}$ and containing the solution γ_{*k} (For $k = 0$ the portion of the orbits with a thin trace should be disregarded.)

Orbit $\gamma_{\alpha,k}$ (winds k times around $\mathbf{0}$)	Time taken by the orbit $\gamma_{\alpha,k}$
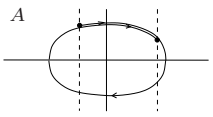	$T_A(\alpha) := 4kT(\alpha) + T_1(\alpha, \phi_0) + T_1(\alpha, \phi_1)$
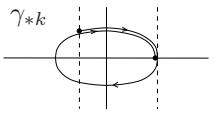	$T_{*k}(\phi_1) := (4k+1)T(\phi_1) + T_1(\phi_1, \phi_0)$
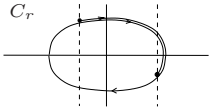	$T_{C_r}(\alpha) := (4k+2)T(\alpha) + T_1(\alpha, \phi_0) - T_1(\alpha, \phi_1)$

Observe that these orbits are analogous to those studied in the previous subsections, which can be considered the case $k = 0$ in this description (i.e., the orbits do not complete a full turn around the origin). The amounts of time spent by each of these orbits are exactly those of the corresponding ones in subsections 3.1.1–3.1.5 with the addition of $4kT(\alpha)$, which is the time of k full turns about the origin.

The following conclusions are easily drawn:

a: From the definitions of the time-maps it follows that $T_k^*(\phi_1) < T_{(k+1)*}(\phi_1)$.

b: From (3.1) we immediately get $T_{k*}(\phi_1) < T_k^*(\phi_1)$.

c: From the results in subsections 3.1.3 and 3.1.4 and the fact that the time spent by the orbits with $k > 0$ is equal the to the time spent by those with $k = 0$ plus $4kT(\alpha)$, we easily conclude that $T_{C_r}(\alpha) > T_{*k}(\phi_1)$ and $T_D(\alpha) > T_k^*(\phi_1)$.

TABLE 2. Branch of solutions to (2.2)-(2.3), with $\phi_0 < \phi_1$, winding k full times around $\mathbf{0}$ and containing the solution γ_k^* (For $k = 0$ the portion of the orbits with a thin trace should be disregarded.)

Orbit $\gamma_{\alpha,k}$ (winds k times around $\mathbf{0}$)	Time taken by the orbit $\gamma_{\alpha,k}$
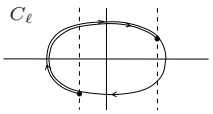	$T_{C_\ell}(\alpha) := (4k+2)T(\alpha) - T_1(\alpha,\phi_0) + T_1(\alpha,\phi_1)$
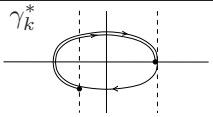	$T_k^*(\phi_1) := (4k+3)T(\phi_1) - T_1(\phi_1,\phi_0)$
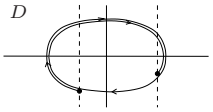	$T_D(\alpha) := 4(k+1)T(\alpha) - T_1(\alpha,\phi_0) - T_1(\alpha,\phi_1)$

d: The study of the relation between $T_{C_\ell}(\alpha)$ and $T_k^*(\phi_1)$, for $\alpha > \phi_1$ sufficiently close to ϕ_1 proceeds exactly as in subsection 3.1.5, paying attention to the fact that we need to add $4kT(\alpha)$ to those computations. Since $T'(\alpha) \to T(\phi_1) \in (0, +\infty)$ as $\alpha \downarrow \phi_1$, and $\tilde{T}''(\tilde{\alpha}) > 0$, the addition of $4kT(\alpha)$ to the right-hand side of (3.3) does nor change the conclusion. Hence we have $T_{C_\ell}(\alpha) < T_k^*(\phi_1)$, for $\alpha - \phi_1 > 0$ sufficiently small. Also, the other conclusions infered from the convexity of $\tilde{\alpha} \mapsto \tilde{T}_{C_\ell}(\tilde{\alpha})$ remain valid.

e: Finally, it remains to study the relation between $T_A(\alpha)$ and $T_{*k}(\phi_1)$. The analysis also follows that presented in subsection 3.1.5. Changings variables as in subsection 3.1.5 we can write an expression for $T_A(\alpha)$ similar to (3.3), namely

$$\begin{aligned} T_A(\alpha) = \tilde{T}_A(\tilde{\alpha}) &:= \\ &:= \quad 2\sqrt{2}k \int_0^{\pi/2} \frac{d\theta}{\sqrt{1-\tilde{\alpha}\sin^2\theta}} + \frac{1}{\sqrt{2}} \int_0^{\phi_0} \frac{dx}{\sqrt{\tilde{\alpha}-\sin^2 x}} + \frac{1}{\sqrt{2}} \int_0^{\phi_0} \frac{dx}{\sqrt{\tilde{\alpha}-\sin^2 x}}. \end{aligned}$$

Now, the convexity argument employed in subsection 3.1.5 and also used in case **d** above, can again be applied to conclude that, for $\alpha - \phi_1 > 0$ sufficiently small, type A orbits satisfy $T_A(\alpha) < T_{*k}(\phi_1)$ and the corresponding branch in the diagram L vs. $y(-L)$ is convex. Note that, in contrast to the case studied in subsection 3.1.5, but as was the case in [1], the branches of type A solutions have a (unique, by convexity) saddle-node, since we know that, from Proposition 2.1, $T_A(\alpha) \to +\infty$ as $\alpha \to \frac{\pi}{2}$.

Thus, we conclude from these results that, for each k, the relation of the various types of orbits among themselves is the same as existed in the case $k = 0$ illustrated in Figure 8. We collect the results obtained thus far in the bifurcation diagram of Figure 9. Observe that, due to the symmetry of the system, the value of $y(-L)$ of the orbits γ_{*k} are the same for all k, and the same happens for γ_k^*; as was the case when $k = 0$, for all k these values in γ_{*k} and in γ_k^* have the same absolute value (and different signs).

3.2. **Case $\phi_0 > \phi_1$.** The analysis of the case $\phi_0 > \phi_1$ proceeds in a way entirely similar to the case $\phi_0 < \phi_1$ and so we will not present the details of the arguments in what follows. We will, in the next figures, exhibit the plots of the several types of orbits and the bifurcation diagram obtained. We start, in Figure 10, by the orbits that, at $t = -L$, satisfy the additional boundary condition $y(-L) = 0$, which we designate by "critical" orbits, as done in the similar situation in subsection 3.1.1.

Due to the symmetry of the problem relative to the transformations $x \mapsto -x$ and $\phi_0 \leftrightarrow \phi_1$, we conclude that, from each "critical" orbit emerges two branches, a subcritical and a supercritical, with exactly the same properties as obtained for the corresponding branches in subsections 3.1.2–3.1.5. These orbits are illustrated in figures 11 and 12.

In an entirely analogous way to what was presented in section 3.1.6, we also have the solution branches corresponding to orbits circling the origin a complete number $k \geqslant 1$ of turns.

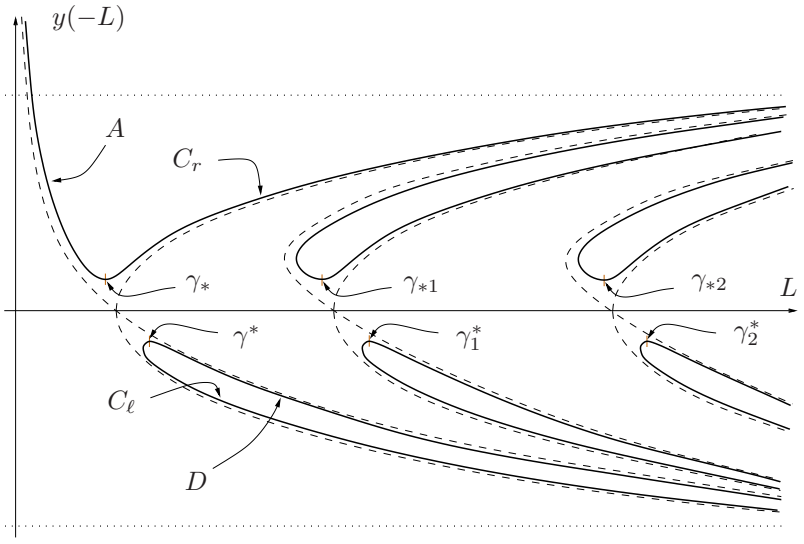

FIGURE 9. Solid lines: portion of the bifurcation diagram when $\phi_0 < \phi_1$ constructed from the analysis presented in subsections 3.1.1–3.1.6. Dashed lines: the corresponding diagram when $\phi_0 = \phi_1$ (from [1]). The designation of the orbits by letters A, C_ℓ, C_r and D correspond to those used in [1]: see Table 1 and Figure 8 of that article.

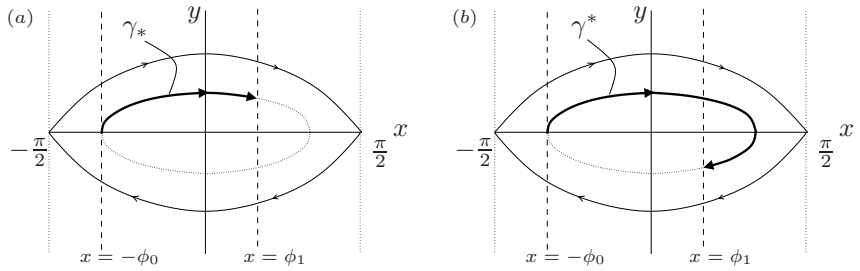

FIGURE 10. Two "critical" orbits of (2.2)-(2.3) with $\phi_0 > \phi_1$: (a) γ_* when $2L = T_* := T(\phi_1) + T_1(\phi_1, \phi_0)$; (b) γ^* when $2L = T^* := 3T(\phi_1) - T_1(\phi_1, \phi_0)$

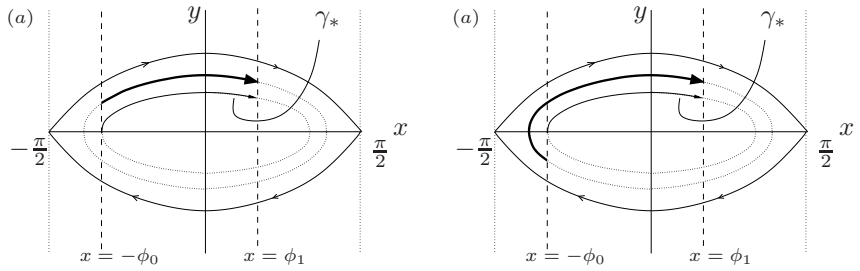

FIGURE 11. Orbits of (2.2)-(2.3), with $\phi_0 > \phi_1$ which are: (a) subcritical relative to the orbit γ_*; (b) supercritical relative to the orbit γ_*.

Collecting these results we can plot the bifurcation diagram corresponding to the case $\phi_0 > \phi_1$. This is done in Figure 13. To understand the apparently drastic difference relative to the diagram for the case $\phi_0 < \phi_1$ presented in Figure 9 we need to bear in mind the fact that in *both* cases what is being plot in the vertical axis is the value of $y(-L)$ of the corresponding orbit. If, in the case $\phi_0 > \phi_1$, we choose to plot the value of $y(L)$ instead, by the symmetry considerations alluded to above, the corresponding bifurcation diagram will be equal to that of Figure 9.

4. Stability analysis of the equilibria

In this section we present a brief study of the stability of the equilibria using the approach of Maginu [6]. We believe it is possible, by a modification of methods originally developed for homogeneous Neumann boundary conditions (see, e.g., [3] and [5, Section 4.3]) to provide more detailed information about the

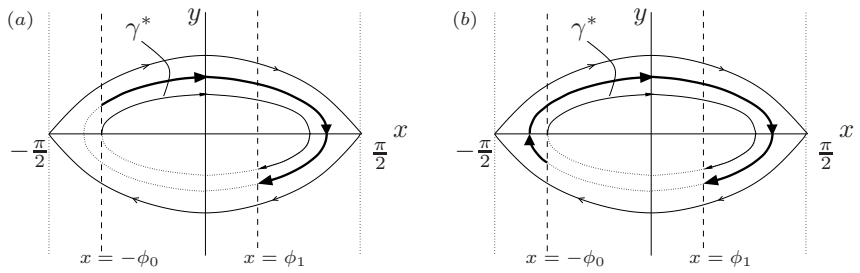

FIGURE 12. Orbits of (2.2)-(2.3), with $\phi_0 > \phi_1$ which are: (a) subcritical relative to the orbit γ^* (for $\alpha - \phi_0 > 0$ sufficiently small); (b) supercritical relative to the orbit γ^*.

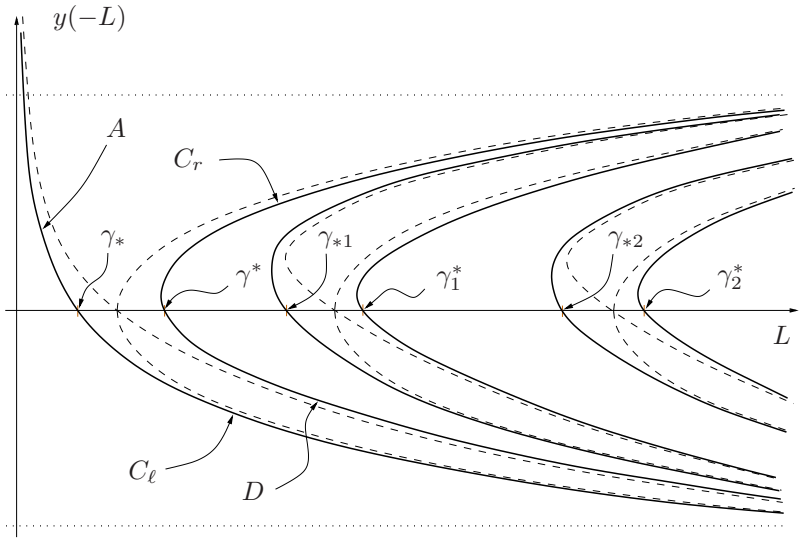

FIGURE 13. Solid lines: portion of the bifurcation diagram when $\phi_0 > \phi_1$ constructed from what was presented and discussed in subsection 3.2. Dashed lines: the corresponding diagram when $\phi_0 = \phi_1$ (from [1]). The designation of the orbits by letters A, C_ℓ, C_r and D correspond to those used in [1]: see Table 1 and Figure 8 of that article.

unstable solutions, in particular clarifying, for each unstable equilibrium, which directions are unstable, and to characterize their heteroclinic connections. This will be postponed to a latter work.

We pretend to classify as stable, asymptotically stable, or unstable the branches of equilibria determined in the last section. The results of [6] relevant to our case are the theorems 3.1, 3.2 and 3.3. What the first two of these theorems state is that solutions $(x(t), y(t))$ of (2.2)–(2.3) are asymptotically stable (as stationary solutions of the corresponding partial differential equation (1.2)–(1.4)) if $y(t)$ has no zeros in $[-L, L)$ or in $(-L, L]$; and it is unstable if $y(t)$ has two or more zeros.

Clearly, these results take care of the stability characterization of all the branches of solutions with $k \geqslant 1$ (they are all unstable), and also when $k = 0$ of the branch denoted by A (which is asymptotically stable), and by D (which is unstable).

Theorem 3.3 of [6] is one of a series or results characterizing the case when $y(t)$ has a single zero in $[-L, L]$, located in $(-L, L)$. Maginus' result states that such an equilibrium E is asymptotically stable if the corresponding time map $T_E(\alpha)$ is strictly increasing, and is unstable if it is strictly decreasing.

Applied to our case, this result will allow us to determine the stability of the remaining cases, namely: the branches C_r and C_ℓ when $k = 0$.

Consider $\phi_0 < \phi_1$. Let us start with the C_r branch. Clearly such solutions are of the type considered in [6, Theorem 3.3] (the existence of a single time instant for which $y(t) = 0$). In Subsection 3.1.3 we concluded that $\frac{dT_{C_r}}{d\alpha} > 0$. Hence, Maginu's result imply the branch is asymptotically stable.

Let us consider now the case of the C_ℓ branch. The relevant computations are the ones in subsection 3.1.5, where we concluded that $T_{C_\ell}(\alpha)$ is convex, with a single local minimum. This means that $\frac{dT_{C_\ell}}{d\alpha} < 0$ for the part of the C_ℓ branch to the left of the γ^* and to the right of the leftmost point of the branch, i.e., the saddle-node bifurcation point (which corresponds to the orbit for which $T_{C_\ell}(\alpha)$ attains its unique minimum.) So, by [6, Theorem 3.3], these equilibria are unstable. For the remaining part of the C_ℓ branch, i.e, for points

of the orbit below the saddle-node bifurcation point, we have $\frac{dT_{C_\ell}}{d\alpha} > 0$, and thus, again by [6, Theorem 3.3], the corresponding equilibria are asymptotically stable.

These stability conclusions for the $k = 0$ branches are collected in Figure 14.

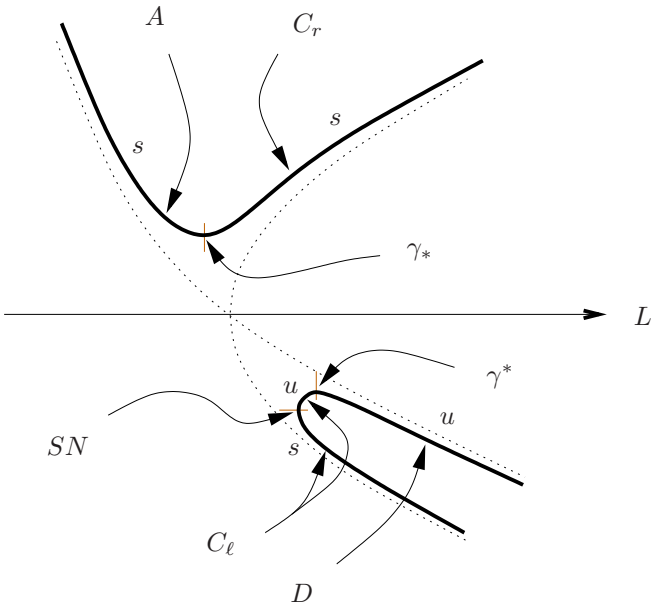

FIGURE 14. Enlargement of the bifurcation diagram of Figure 8. The saddle-node bifurcation point refered to in the text is denoted by SN, and the letters s and u denote branches of stable and unstable solutions, respectively. The remaining notation is as in Figure 8.

Exactly the same results can be applied to the case when $\phi_0 > \phi_1$ with analogous results: by theorems 3.1 and 3.2 of [6] all the $k \geqslant 1$ branches are unstable, as well as the D branch, whereas the A branch is asymptotically stable. An analysis corresponding to that in subsections 3.1.3 and 3.1.5 and the application of theorem 3.3 of [6] results in the conclusion that C_ℓ is an asymptotically stable branch, and the portion of the C_r branch between y^* and the leftmost point (a saddle-node) of the branch corresponds to unstable equilibria, whereas the points above this last point are asymptotically stable equilibria.

These conclusions about the stability of the $k = 0$ branches are collected in Figure 15.

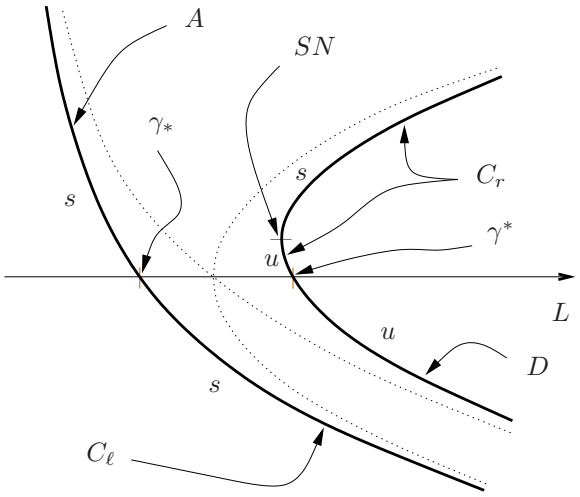

FIGURE 15. Enlargement of the bifurcation diagram of Figure 13. The saddle-node bifurcation point refered to in the text is denoted by SN, and the letters s and u denote branches of stable and unstable solutions, respectively. The remaining notation is as in Figure 13.

References

1. F.P. da Costa, E.C. Gartland, Jr., M. Grinfeld, J.T. Pinto, *Bifurcation analysis of the twist-Fréedericksz transition in a nematic liquid-crystal cell with pre-twist boundary condition*, Eur. J. of Appl. Math., **20** (2009) 269–287.
2. F.P. da Costa, M. Grinfeld, N. Mottram, J.T. Pinto, *Uniqueness in the Freedericksz transition with weak anchoring*, J. Differential Equations, **246**, (2009) 2590–2600.
3. B. Fiedler, C. Rocha, *Heteroclinic orbits of semilinear parabolic equations*, J. Differential Equations, **125** (1), (1996) 239–281.
4. V. Fréedericksz, A. Repiewa, *Theoretisches und Experimentelles zur Frage nach der Natur der anisotropen Flüssigkeiten*, Z. f. Phys., **42** (7), (1927) 532–546.
5. J.K. Hale, *Asymptotic Behavior of Dissipative Systems,* Mathematical Surveys and Monographs, number 25, American Mathematical Society, Providence, RI, 1988.
6. K. Maginu, *Stability of stationary solutions of a semilinear parabolic partial differential equation*, J. Math. Anal. Appl., **63** (1978) 224–243.
7. I.W. Stewart, *The Static and Dynamic Continuum Theory of Liquid Crystals,* The Liquid Crystals Book Series, vol. 2, Taylor & Francis, London, 2004.
8. D.-K. Yang, S.-T. Wu, *Fundamentals of Liquid Crystal Devices,* 2nd Ed., Wiley-SID Series in Display Technology, John Wiley & Sons, Chichester, 2015.

E-mail address: fcosta@uab.pt
E-mail address: misabel.mendezaller@educa.madrid.org
E-mail address: jpinto@math.tecnico.ulisboa.pt